Safe Arm Design with MR-based Passive Compliant Joints and Visco-elastic Covering for Service Robot Applications

Seong-Sik Yoon
Intelligent Systems Institute, National Institute of Advanced Industrial Science and Technology, 1-1-1 Umezono, Tsukuba-shi Ibaraki, 305-8568 Japan
Sungchul Kang*, Seung-kook Yun, Seung-Jong Kim
Intelligent Robotics Research Center and Tribology Research Center, Korea Institute of Science and Technology, Hawolgok-dong 39-1, Sungbuk-ku, Seoul 136-791, Korea
Young-Hwan Kim
Intelligent Mechanical System Research Department, Electro-Mechanical Research Institute Hyundai Heavy Industries Co., Ltd., Mabuk-ri, Kuseong-myun, Yongin-shi, Kyunggi-do 449-716, Korea
Munsang Kim
Intelligent Robotics Research Center, Korea Institute of Science and Technology, Hawolgok-dong 39-1, Sungbuk-ku, Seoul 136-791, Korea

In this paper a safe arm with passive compliant joints and visco-elastic covering is designed for human-friendly service robots. The passive compliant joint (PCJ) is composed of a magneto-rheological (MR) damper and a rotary spring. In addition to a spring component, a damper is introduced for damping effect and works as a rotary viscous damper by controlling the electric current according to the angular velocity of spring displacement. When a manipulator interacts with human or environment, the joints and cover passively operate and attenuate the applied collision force. The force attenuation property is verified through collision experiments showing that the proposed passive arm is safe in view of some evaluation measures.

Key Words : Safety, Service Robot, Passive Compliant Joint, Magneto-rheological Fluid, Visco-elastic Covering

Nomenclature

A_C : Contact area of a cover
A, A_O : Cross sectional areas
$a(t)$: Acceleration felt by a human at time t
a_{slope} : Slope defined between applied current and generated torque
B : Viscous damping coefficient
$B_{1i}, B_{1o}, B_{2i}, B_{2o}$: Flux densities acting on each sectional area
$B_{\max}$: Maximum viscous damping coefficient
h : Height of piled coil bundle
d_s : Geometric design parameter in stator part
d_r : Thickness of a disk
F : Impact force
F_{human} : Force acting on a human
F_{limit} : Acceptable pain tolerance limit
$F_{1i}, F_{1o}, F_{2i}, F_{2o}$: Shear forces acting on each sectional area
G_c : Elastic modulus of a cover (Pas)
G^i : Gravity term in arm dynamics for the i-th axis

* Corresponding Author,
E-mail : kasch@kist.re.kr
TEL : +82-2-958-5589; **FAX** : +82-2-958-5629
Intelligent Robotics Research Center, Korea Institute of Science and Technology, Hawolgok-dong 39-1, Sungbuk-ku, Seoul 136-791, Korea. (Manuscript **Received** December 29, 2003; **Revised** August 11, 2004)

I : Current applied to coil
J_{max} : Maximum moment of inertia
K : Torsional stiffness of spring
K_P, K_I, K_D : Proportional, integral, derivative control gains
k : Spring constant of each small spring
M_R : Effective mass of a robot arm
M_H : Upper part mass of a human
N : Turn number of coil
n_K : Number of small springs
R_s, R_{mri}, R_{mro} : Reluctances of the stator part, left MRF, right MRF
$r_{1i}, r_{2i}, r_{1o}, r_{2o}$: Distances from center line in radial direction
SI : Severity index
$T_{gravity}$: Torque considering maximum gravitational effect of each joint
x_H : Displacement of a human
x_R : Displacement of a robot
Z_c : Thickness of a cover (m)

Greek symbols

η_c : Viscous coefficient of a cover (Pa)
δ : Gap filled by MR fluid
$\mu_0, \mu_{rf}, \mu_{rs}$: Permeability of free space, the relative permeabilities of MR fluid and steel
ϕ_{sat} : Saturated magnetic flux in a disk part
ϕ : Magnetic flux
τ_B : Experimentally obtained torque of MR damper
$\tau_{B\,max}$: Desired maximum torque of damper
τ_m : Motor torque considering reduction ratio
τ_T : Theoretically calculated resultant torque of MR damper
θ_d : Desired angle of joint
$\bar{\theta}_d$: Modified desired angle considering deflection by gravity in steady state
θ_L : Angle between current link and next link
θ_m : Angle of motor
θ_{max} : Maximum deflection angle of spring
$\dot{\theta}_{max}$: Maximum angular velocity of spring
θ_r : Angle sensed by resolver
ζ_{max} : Desired damping ratio determined by taking account of overshoot and interaction with human

Subscripts

B : Viscous damping
c : Contact
D : Derivative
d : Desired
$gravity$: Gravity
$human$: Human
I : Integral
i : Inner part
O : Outer part
P : Proportional
$limit$: Limit
max : Maximum
mri : Inner part of MRF
mro : Outer part of MRF
rf : Value of MR fluid relative to free space
rs : Value of steel relative to free space
R : Robot
r : Rotor part
s : Stator part
sat : Saturated
K : Spring
$slope$: Slope
T : Theoretically
0 : Free space

Superscripts

i : The i-th axis

1. Introduction

Robots are recently expected to provide various kinds of service directly to human in human-robot coexisting environment. From the viewpoint of human-robot interaction, safety is one of the most important issues to be accomplished (Yamada et al., 1997 ; Ikuta and Nokata, 1999 ; Lim and Tanie, 2000). Giving compliance to a robot arm is being thought to be a good way to greatly enhance the safety issues. There generally exist two strategies to realize the robot compliance : active and passive. Active compliance approach usually makes use of the feedback signals from force/torque sensors equipped either on a robot hand or at link joints so that the robot controller can detect the applied external force and give a proper response (Albu-Shaffer and

Hirzinger, 2002). The active compliance approach generally has limitations in delayed control and incomplete safety in case of electrical malfunctioning, even though it can offer a high programming ability for compliance control. Thus manipulators with active compliance function may cause either damage to human or failure of power transmission due to shock when unexpected contact occurs. On the other hand, passive compliance can be realized by adopting a passive mechanism to produce an appropriate reaction to the applied forces without time-delay and electrical malfunctioning.

Among previous approaches for passive compliance mechanisms, in (Yamada et al., 1997) a visco-elastic cover is used for the passive compliance and a safety condition by impact force in unexpected collision is suggested. Here an arm is called "safe" if the following condition about the impact force F is satisfied :

$$F \leq F_{limit} \tag{1}$$

which implies that an acceptable pain tolerance limit is F_{limit}. But in (Yamada et al., 1997) no passive compliant joint is used. Next, a passive trunk mechanism is developed in (Lim and Tanie, 2000) where it consists of linear springs and dampers between a mobile part and an arm. By the way, these joints are not rotary type joints. Here a visco-elastic cover is also used like in (Yamada et al., 1997). Lastly, the mechanical impedance adjuster is developed in (Morita and Sugano, 1995) where a variable spring and a damper by an electromagnetic brake are used for the passive compliant joint of the Wendy robot arm (Iwata et al., 1999). By the way, the electromagnetic brake has problems such as hysteresis, clanking noise at the contact time of a disk, and frictional wear. In (Morita and Sugano, 1995), a visco-elastic cover is also used for the attenuation of an impact force like in (Yamada et al., 1997) and (Lim and Tanie, 2000). From the approaches introduced until now, we can see that both passive complaint joints and a cover are used for the safety of a robot arm.

Now magneto-rheological fluid to be used in this research is explained. Recently magneto-rheological (MR) fluid has attracted researchers' attention as a smart material (Carlson et al., 1996 ; Jolly et al., 1998 ; Jung and Park, 1999 ; Kim and Oh, 2001 ; Oh and Onoda, 2002). The MR fluid is suspension of micro-sized, magnetizable particles in a carrier fluid. Altering the strength of an applied magnetic field precisely controls the yield stress of the fluids. A rotary MR damper with viscous damping property can be implemented by controlling the applied current. And the MR fluid has broad operational temperature range, and fast response time, and high dynamic yield stress. An MR damper using the MR fluid has the following advantages. First, it consumes less power and has less hysteresis than an electromagnetic damper. And also it can do smoother and quieter operation than an electromagnetic damper. Secondly, variable damping control is possible. Finally by simple and modular designs, power ratios versus weight and size can be increased. Therefore in this research, we want to design a new passive compliant joint (PCJ) with a rotary MR damper with advantages mentioned and a rotary spring.

In this work we use the safety condition by impact force in unexpected collisions between a human and a robot (Yamada et al., 1997). From the studies in (Yoshida et al., 1995) and (Walker, 1994) about impact dynamics, we can see that factors generating an impulse are the mass, velocity, and joint torque of the arm. Thus to make an arm meet the safety condition Eq. (1), we should basically make a light arm with passive compliant joints and covering, or schedule the velocity according to the inertia matrix. This is a motivation of this work to develop an arm with passive compliant joints and visco-elastic covering.

In this paper, a safe arm with passive compliant joints and visco-elastic covering for human-friendly service robots is presented. The passive compliant joint (PCJ) is newly designed to have a compact integrated structure with a magneto-rheological damper and a spring. The rotary spring gives the arm compliant property, but also it might be a source of vibration. Therefore the damper is introduced for damping effect and

works as a rotary viscous damper by controlling the electric current according to the angular velocity of spring displacement. In unexpected collisions, the joints and cover passively attenuate the applied collision force. The force attenuation property of the developed arm is verified through collision experiments showing that the proposed passive arm is safe in view of some evaluation measures.

2. Safe Arm Design

In this section, firstly a passive compliant joint with a magneto-rheological damper and a spring is developed. Second a soft cover is selected. Finally a six-dof arm with the PCJs and cover is designed.

2.1 Passive compliant joint design

The design of a passive compliant joint is depicted in Fig. 1. It consists of a magneto-rheological (MR) rotary damper, a rotary spring for elasticity. The rotary spring has compliant property, but also it might be a source of vibration. Therefore the damper is introduced for damping effect and implemented by using MR fluid. The PCJ has a resolver sensor with 16-bits high resolution to read the relative position between a housing and a next link due to the spring displacement. The relative position is converted into a relative velocity signal by a numerical differentiation and a filtering and is sent to a damping tuner which converts Coulomb friction property of the MR fluid into viscous one. Note that the damper and spring are located in parallel between the housing and next link.

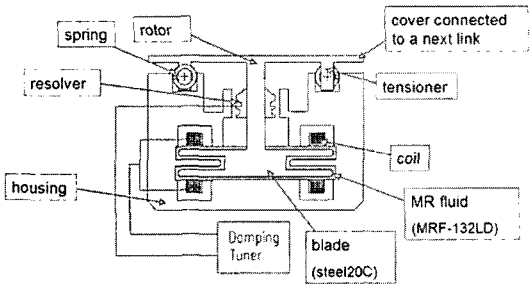

Fig. 1 Design of passive compliant joint mechanism

Firstly, an MR damper is developed and the experimental tests to the dampers are presented. As shown in Fig. 2, two disks and coils are located in the axial direction because the joints of an arm have margin to the axial direction but a little margin to the radial direction. The hatched area represents MR fluid (MRF) in the narrow gap. We use the MRF-132LD (Lord corporation, 1999). Consider the case that current flows in both coils. Then all magnetic flux through the paths is generated as shown in Fig. 2. And its magnetic circuit considering saturation effects of the disk parts can be obtained as shown in Fig. 3. The reluctance equations for the circuit in Fig. 3 are formulated as follows:

$$R_s=\frac{h+d_s/2}{\mu_0\mu_{rs}}\left(\frac{1}{A_i}+\frac{1}{A_o}\right)+\frac{(r_{1o}+r_{2o}-r_{1i}-r_{2i})/2}{\mu_0\mu_{rs}\cdot 2\pi d_s(r_{1o}+r_{2i})/2} \quad (2)$$

$$R_{mri}=\frac{\delta}{\mu_0\mu_{rf}A_i},\ R_{mro}=\frac{\delta}{\mu_0\mu_{rf}A_o}$$

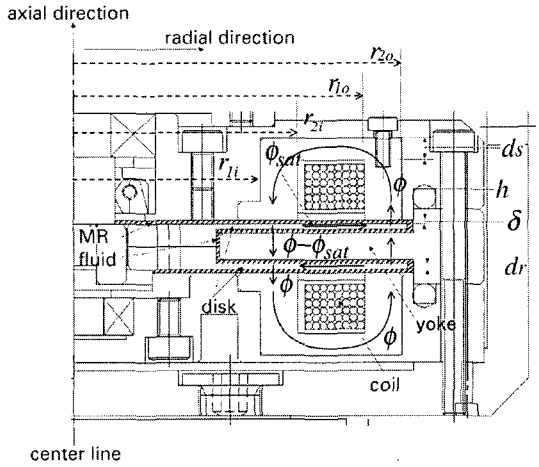

Fig. 2 A sectional view of the damper for explaining fluxes in the case that current flows in both coils

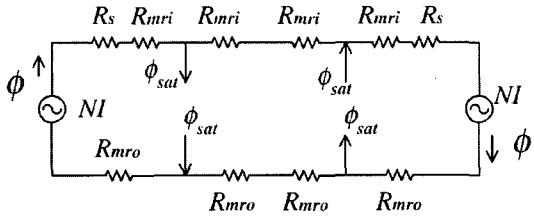

Fig. 3 A magnetic circuit considering saturation effects

where R_s, R_{mri}, R_{mro} are the reluctances of the stator part, left MRF, right MRF, respectively. And δ, h, d_s, d_r, r_{1i}, r_{1o}, r_{2i}, r_{2o} are geometric design parameters for the reluctances, $\mu_0(=4\pi\times 10^{-7})$, $\mu_{rf}(=6.51)$, $\mu_{rs}(=1470)$ are the permeability of free space, the relative permeabilities of the MR fluid and steel (Lord materials division, 1999; Jung and Park, 1999), and the sectional areas A_i, A_o are calculated as:

$$A_i=\pi(r_{2i}^2-r_{1i}^2),\ A_o=\pi(r_{2o}^2-r_{1o}^2) \tag{3}$$

The resultant torque of the damper can be theoretically calculated from the following equation:

$$\begin{aligned}\tau_T=&[(r_{1i}+r_{2i})\times(F_{1i}+F_{2i})\\&+(r_{1o}+r_{2o})\times(F_{1o}+F_{2o})]\end{aligned} \tag{4}$$

where shear forces acting on each sectional area are as follows:

$$\begin{aligned}F_{1i}&=80000B_{1i}A_i-10000A_i\\F_{1o}&=80000B_{1o}A_o-10000A_o\\F_{2i}&=80000B_{2i}A_i-10000A_i\\F_{2o}&=80000B_{2o}A_o-10000A_o\end{aligned} \tag{5}$$

and B_{1i}, B_{1o}, B_{2i}, B_{2o} are flux densities acting on the each sectional area. Note that Eq. (5) is approximately obtained form the date of the Lord corporation as shown in Fig. 4. The saturated flux density in the disk part is 1.5 (tesla) (Lord materials division, 1999). Thus the saturated magnetic flux in the disk part

$$\phi_{sat}=1.5\times 2\pi r_{2i}d_r \tag{6}$$

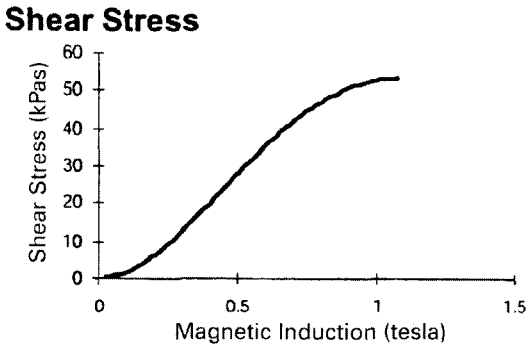

Fig. 4 Shear stress versus magnetic flux density of the MRF-132LD (Lord corporation, 1999)

By the Kirchoffs's Law for the magnetic circuit,

$$NI=\phi(R_s+R_{mr})+(\phi-\phi_{sat})R_{mr} \tag{7}$$

where N is turn of coil, I is current applied to the coil, ϕ is magnetic flux and

$$R_{mr}=\frac{\delta}{\mu_0\mu_{rf}}\left(\frac{1}{A_i}+\frac{1}{A_o}\right) \tag{8}$$

Thus

$$\phi=\frac{NI+R_{mr}\phi_{sat}}{R_s+2R_{mr}} \tag{9}$$

Finally, the flux densities acting on the each area are calculated as:

$$\begin{aligned}&B_s=\phi/(2\pi r_{2i}d_s),\ B_{1i}=\phi/A_i,\ B_{1o}=\phi/A_o\\&B_{2i}=(\phi-\phi_{sat})/A_i,\ B_{2o}=(\phi-\phi_{sat})/A_o\end{aligned} \tag{10}$$

Note that the resultant theoretical torque is calculated from Eq. (4).

We make three dampers as shown in Fig. 5 for the three joints in the lower part of an arm to be introduced in the sec. 2.3. The numerical parameter values of the dampers can be obtained in (Kim et al., 2002). The actual relations between generated torque and applied current are experimentally obtained through a setup using an F/T sensor (Kim et al., 2002). The test results are almost linear as shown in Fig. 6. Resultantly, we can see that the theoretical torques from Eq. (4) and experimental torques of the dampers coincides with each other. The detailed numerical values of the torques can be obtained in (Kim et al., 2002).

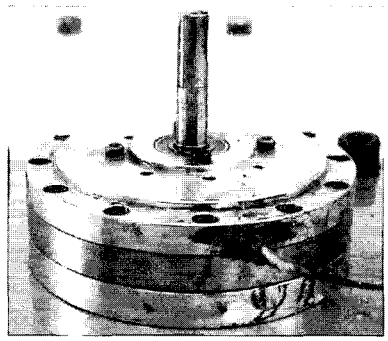

Fig. 5 The picture of an implemented damper

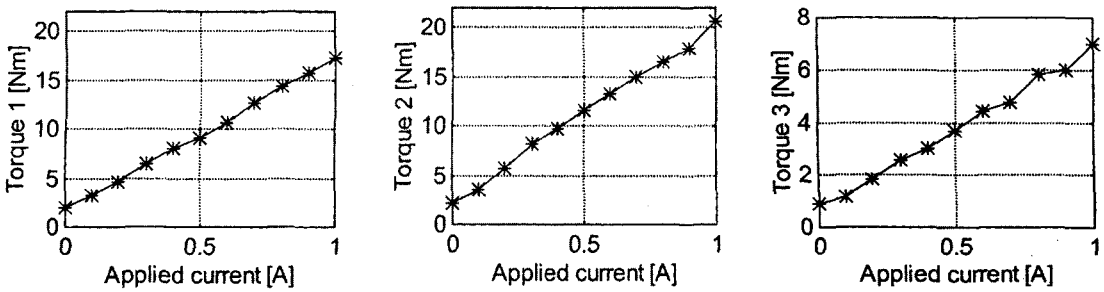

Fig. 6 Relations between damping torques and applied currents of the MR dampers

Now, a technique to tune the damping coefficient is addressed. Originally, the rotary dampers have the Coulomb friction properties, that is, the torque is proportional to the applied current. Thus the relation between the applied current I and torque τ_B of the damper can be approximately represented as follows:

$$\tau_B = a_{slope} I \times sign(\dot{\theta}_r) \tag{11}$$

where a_{slope} is the slope obtained from Fig. 6. Note that a viscous damper should satisfy the following relation:

$$\tau_B = B\dot{\theta}_r \tag{12}$$

where B is a viscous damping coefficient and θ_r $(\theta_L - \theta_m)$ is a relative angle between the link and the housing. Therefore if we control the current by the following rule

$$I = \frac{B}{a_{slope}} |\dot{\theta}_r| \tag{13}$$

the damper can have the viscous damping property Eq. (4). Notice that this property is approximately derived.

Secondly, the spring components are explained. Fig. 7 shows a three-dimensional model of the spring component. The upper part and lower part are assembled and rotated relatively. The torsional stiffness of the spring component is calculated as follows:

$$K = n_K k \ (\text{Nm/rad}) \tag{14}$$

where k is the spring constant of each small spring and n_K is the number of the small springs. Note that the number of the small springs can be tuned. The implemented parameters are given in (Kim et al., 2002).

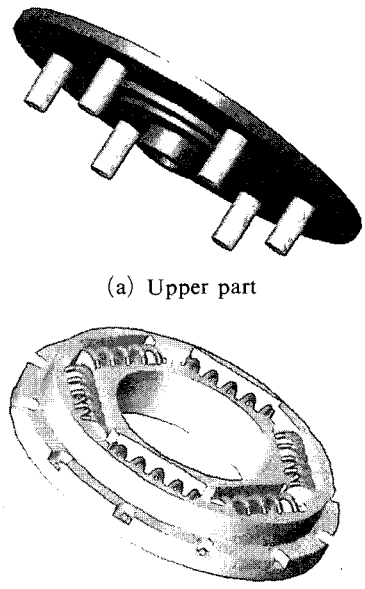

(a) Upper part

(b) Lower part

Fig. 7 A three-dimensional model of the spring component

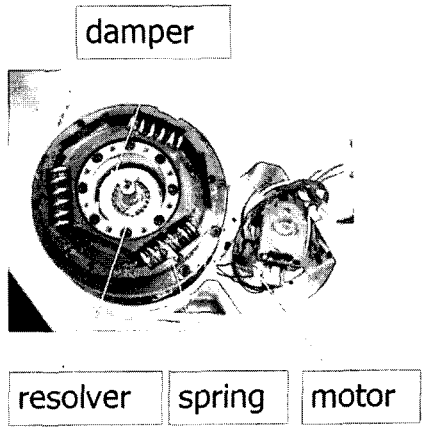

Fig. 8 A picture of the passive compliant joint

Finally, a passive compliant joint with the spring and damper is obtained as shown in Fig. 8 where the two components build a parallel structure. The passive joint is used for the three joints in the lower part of an arm.

2.2 Visco-elastic cover design

In this subsection a visco-elastic cover to attenuate a collision force is addressed. The cover can be modeled simply by a spring and a damper as shown in Fig. 9. If a robot arm is represented by a simple body with a mass M_R and the arm collides with a human, the collision model is obtained as:

$$\begin{aligned} M_R\ddot{x}_R + F_{human} &= 0 \\ M_H\ddot{x}_H - F_{human} &= 0 \end{aligned} \tag{15}$$

where

$$\begin{aligned} F_{human} &= B_u(\dot{x}_R - \dot{x}_H) + K_u(x_R - x_H) \\ B_u &= \frac{A_c\eta_c}{Z_c},\ K_u = \frac{A_cG_c}{Z_c} \end{aligned} \tag{16}$$

M_R is the effective mass of a robot arm, M_H is the upper part mass of a human, F_{human} is force acting on a human, x_R is the displacement of the robot, x_H is the displacement of the human, A_C is the contact area of the cover, η_C, G_C, Z_C are the viscous coefficient (Pa), elastic modulus (Pas), and thickness of the cover (m), respectively. Through some impact simulations using the collision model, the Urethan foam PORON SR-L-24 made in the INOAC corporation is selected for the cover among several materials, which attenuates impact force to a human below a pain tolerance limit (Yamada et al., 1997) and has a high percentage of absorbency of impact momentum. The thickness of the cover is decided by taking account of the increase in the size of the arm.

2.3 Safe arm design

In this subsection, a safe arm with the MR-based passive compliant joints and the visco-elastic covering developed in previous subsections is designed for service robot applications. A six-dof safe arm with 3 Kg-payload, 30 kg weight and 1 m reach has been developed as depicted in Fig. 10. This arm is used for the PSR-2 (Public Service Robot) developed at the KIST (Korea Institute of Science and Technology). Taking account of the weight increase of the arm due to the weight of MR dampers and springs, PCJs are adopted only to three joints in the lower part of the 6-dof service robot arm. The three PCJs give the arm compliance into the three directions. Main parameters for the PCJs are determined by the following criterion. Firstly the parameter K of the springs is determined by the following equation considering deflection due to gravitational load for the corresponding joint:

$$K = 1.5\,T_{gravity}/\theta_{\max} \tag{17}$$

where $T_{gravity}$ is the torque considering maximum gravitational effect of each joint. That is, K is determined so that the maximum deflective angle can be $\theta_{\max}$ when a torque 1.5 times than

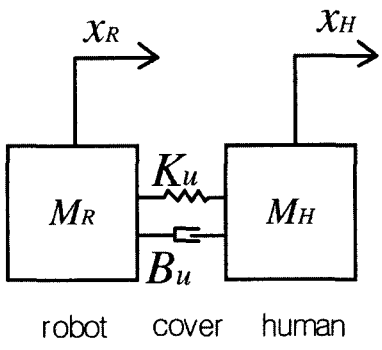

Fig. 9 A simplified diagram for modeling a visco-elastic cover

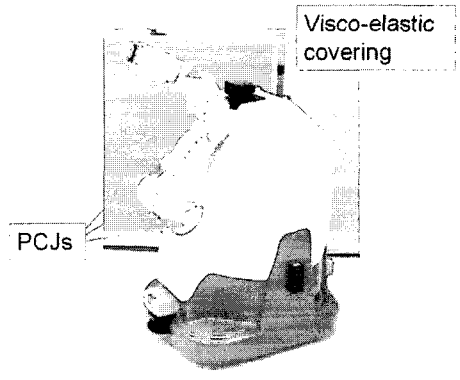

Fig. 10 The developed safe arm and mobile robot

Table 1 SPEC of each PCJ

	Axis number		
	Axis 1	Axis 2	Axis 3
Spring constant (Nm/rad)	350	420	210
Maximum damping torque (Nm)	17.3	20.5	6.97
Viscous damping coefficient (Nm sec/rad)	30.0	35.7	11.3

the gravitational torque is applied to a joint. Secondly, $B_{\max}$ is set so that the following characteristic equations can be matched :

$$s^2+\frac{B_{\max}}{J_{\max}}s+\frac{K}{J_{\max}}=0$$
$$s^2+2\zeta_{\max}w_n s+w_n^2=0 \tag{18}$$

where damping ratio $\zeta_{\max}$ is determined by taking account of overshoot and interaction, where $J_{\max}$ is the maximum moment of inertia. That is,

$$B_{\max}=2\zeta_{\max}\sqrt{J_{\max}K} \tag{19}$$

Thus the required maximum torque of the damper

$$\tau_{B\,\max}=B_{\max}\dot{\theta}_{\max} \tag{20}$$

where $\dot{\theta}_{\max}$ is the maximum angular velocity. The main parameters for the PCJs are shown in Table 1.

3. Controller Design with Gravity Compensation

The safe robot arm has a distributed control architecture based on the CAN (controller area network) bus. Thus it is desirable to control each axis independently using a simple control law. In (Yoon et al., 2002), a model of one-dof arm with a PCJ is introduced and its controllability is analyzed. The analytical result is that as long as K is not zero the determinant of the controllability matrix is not zero, and thus the system is always controllable regardless of the viscous damping coefficient.

Now, a method to control the positions of the three PCJs is proposed. The objective of the control is to have the following regulating performance

$$\lim_{t\to\infty}\{\theta_L^i(t)-\theta_d^i\}=0,\ i=1,\ 2,\ 3 \tag{21}$$

without the loss of passive compliance property of the spring and damper, where θ_d^i is a constant desired angle for the i-th joint, θ_L^i is a angle between a current link and the next link for the i-th joint. The three passive joints are deflected by gravity if the following PID control law without gravity compensation is used :

$$\tau_m^i=-K_P^i(\theta_m^i-\theta_d^i)-K_D^i(\dot{\theta}_m^i-\dot{\theta}_d^i)$$
$$-K_I^i\int_{t_0}^{t}(\theta_m^i-\theta_d^i)\,d\tau \tag{22}$$

where τ_m^i is a motor torque considering the reduction ratio and θ_m^i is a angle of the motor. Note that the following relation is obtained :

$$\theta_L^i=\theta_m^i+\theta_r^i \tag{23}$$

where θ_r^i is an angle sensed by the i-th resolver. To compensate for position error due to the gravity in steady state, the following control method similar to that for the passive joint called the MIA (Morita and Sugano, 1995) is used :

$$\tau_m^i=-K_P^i(\theta_m^i-\bar{\theta}_d^i)-K_D^i(\dot{\theta}_m^i-\dot{\bar{\theta}})$$
$$-K_I^i\int_{t_0}^{t}(\theta_m^i-\bar{\theta}_d^i)\,d\tau \tag{24}$$

where

$$\bar{\theta}_d^i=\theta_d^i+G^i(\theta_d^1,\ \cdots,\ \theta_d^6)/K^i,\ i=1,\ 2,\ 3 \tag{25}$$

K_P^i, K_I^i, K_D^i are proportional, integral, derivative control gains for the i-th axis, G^i means the i-th term related to gravity in the arm dynamics, and K^i represents a spring constant for the i-th axis. This control method has an advantage to obtain the passive compliance property during position control because the spring and damper can be passively operated, and yet has a disadvantage that the method is sensitive to modeling errors. By the way, notice that if we use the following control method

$$\tau_m^i=-K_P^i(\theta_L^i-\theta_d^i)-K_D^i(\dot{\theta}_L^i-\dot{\theta}_d^i)$$
$$-K_I^i\int_{t_0}^{t}(\theta_L^i-\theta_d^i)\,d\tau \tag{26}$$

the position control mode and passive compliance mode are not explicitly separated and the passivity which is an advantage of the PCJ is not fully used. Therefore we don't use Eq. (26) but Eq. (24) to control the PCJ.

4. Experimental Results

In this section, the evaluation of safety and damping effects of the developed arm is accomplished through experiments.

4.1 Programmable damping effects of the passive compliant joints

The damping effects are evaluated in a posture where the only third joint is set to passive compliant joint as shown in Fig. 11. The first and second axes are fixed and also the input of the harmonic drive of the third axis is fixed. Initially the third joint is set to about 8.3 (deg) and then released. The resulting responses according to the change of B are obtained as represented in Fig. 12. As the visco-damping coefficient increases, the angle sensed by the 3rd resolver decreases. In steady-state the angle converges to about −3.1 (deg) due to gravity.

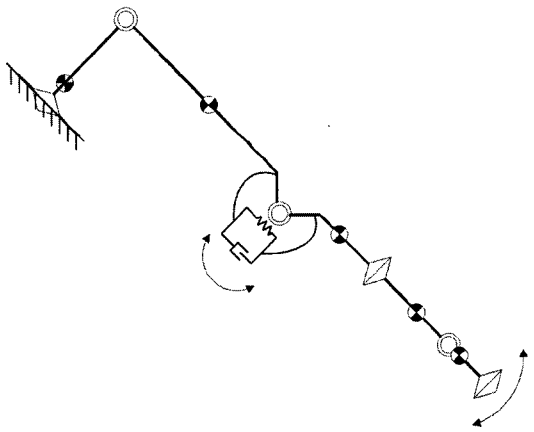

Fig. 11 Posture for a test of damping effects

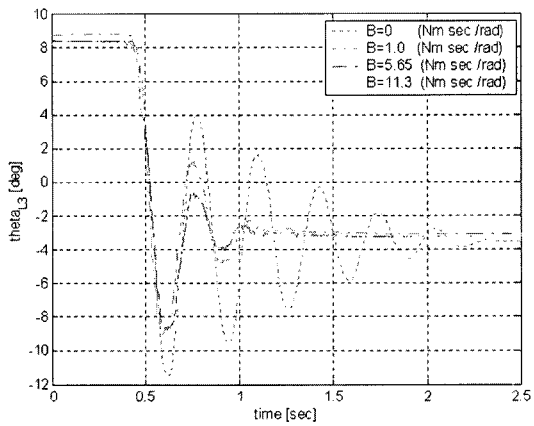

Fig. 12 Damped results according to the change of viscous damping coefficient B

4.2 Safety evaluation through impact experiments

Impact experiments are accomplished under the condition where linear velocity is set to 0.2 and 0.5 (m/sec), and M_H=9.3 (Kg) considering the effective mass of human upper part in a posture as shown in Fig. 13. The mass collides to the end-

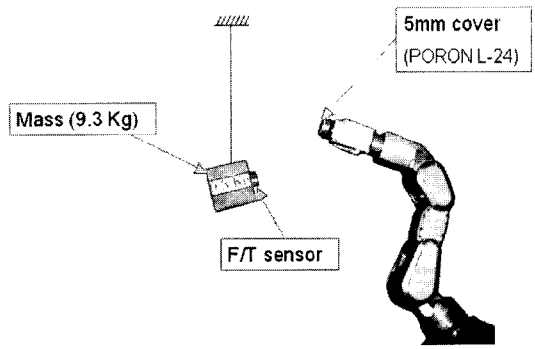

Fig. 13 Initial posture for impact experiments

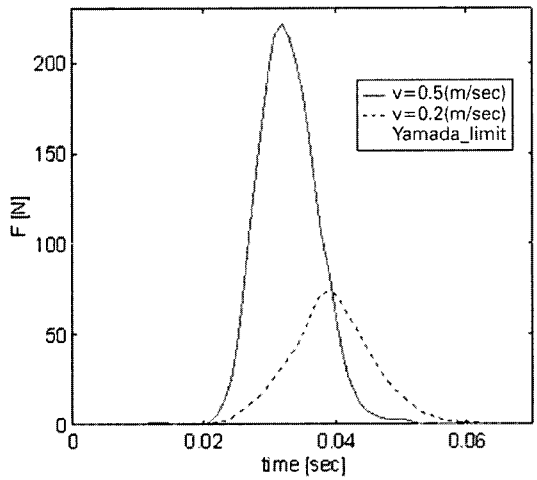

Fig. 14 Measured impact forces

effector of the manipulator which is covered with soft covering. As seen in Fig. 14, impact forces are measured by an F/T sensor, where the solid line indicates impact force in case of 0.5 (m/sec), the dotted line represents impact force in case of 0.2 (m/sec), and the dash-dotted line indicates the middle pain tolerance limit 100 (N) obtained in (Yamada et al., 1997). In case of 0.2 (m/sec), the peak force 71 (N) is less than the middle limit. Next, the severity index (Society of Automotive Engineers, 1999) is calculated to 1.8 by the following equation:

$$SI=\int_0^t a(\tau)^{2.5}d\tau \tag{27}$$

where $a(t)=F(t)/M_H$ and an SI value 400 implies the limit of concussion of the brain (Morita et al., 1998). Therefore in view of the two criteria, the arm is safe. Under the condition 0.5 (m/sec), the peak force 212 (N) is greater than the middle limit. Thus the arm is not safe by the Yamada's criterion. But the SI value is calculated to 19 less than 400. Therefore we can see that in view of the severity index the arm is safe in case of 0.5 (m/sec), but in view of the Yamada's criterion the arm is safe only when the impact velocity is less than about 0.25 (m/sec).

5. Conclusions

In this paper, we propose a new safe arm with passive compliant joints with springs and dampers and a soft covering for human-robot interaction. The spring component can attenuate force to be applied to a human. A developed joint has a feature that magneto-rheological dampers are used. The dampers play a role of suppressing the vibration from the rotary spring. An efficient tuning method to convert the Coulomb friction property of the dampers into a viscous damping one and a position control method with gravitational compensation are proposed. By simulations using a simplified model, a visco-elastic cover is selected, which attenuates impact force to a human below a pain tolerance limit and has a high percentage of absorbency of impact momentum. Finally, force attenuation and damping effects of vibration of the arm have been verified through experiments. And the safety of the developed arm is discussed in view of a pain tolerance limit and severity index. By the way, the joint increases weight by three kilograms per one joint. Thus as a future research, a lighter passive compliant joint will be developed. As described in (Yoshida et al., 1995) and (Walker, 1994) about impact dynamics for rigid joint arms, the theoretical studies about impact dynamics for passive compliant joint arms are needed. These theoretical results will give good bases for the design of passive compliant joints and the analysis for impact experiments.

Acknowledgments

This paper was supported in part by the Ministry of Science and Technology in the Republic of Korea and in part by the Korea Research Foundation Grant funded by Korea Government (MOEHRD, Basic Research Promotion Fund) (No.M01-2003-000-20018-0).

References

Albu-Shaffer, A. and Hirzinger, G., 2002, "Cartesian Impedance Control Techniques for Torque Controlled Light-Weight Robots," *Proc. of the IEEE International Conference on Robotics and Automation*, pp. 657~663.

Carlson, J. D., Catanzarite, D. M. and St. Clair, K. A., 1996, "Commercial Magneto-rheological Fluid Devices," *Proc. of Electro-Rheological, Magneto-Rheological Suspensions and Associated Technology*, W. Bullough, Ed., World Scientific, Singapore, pp. 20~28.

Ikuta, K. and Nokata, M., 1999, "General Evaluation Method of Safety for Human-care Robots," *Proc. of the IEEE International Conference on Robotics and Automation*, pp. 2065~2072.

Iwata, H., Hoshino, H., Morita, T. and Sugano, S., 1999, "A Physical Interference Adapting Hardware System Using MIA and Humanoid Surface Covers," *Proc. of IEEE/RSJ International Conf. on Intelligent Robots and Systems*,

pp. 1216~1221.

Jolly, M. R., Bendor, J. W. and Carlson, J. D., 1998, "Properties and Applications of Commercial Magnetorehological Fluids," *Proc. of SPIE 5th Annual Int. Symposium on Smart Stucures and Materials*.

Jung, B. -B. and Park, Y., 1999, "Electronically Controlled Power Steering by Magneto-rheological Fluid," *Proc. of Korea Automatic Control Conference*, pp. 1173~1176.

Kim, J. -H. and Oh, J. -H., 2001, "Development of an Above Knee Prothesis Using MR Damper and Leg Simulator," *Proc. of the IEEE International Conference on Robotics and Automation*, pp. 3686~3691.

Kim, M., Yoon, S. -S., Kang, S., Kim, S. -J., Kim, Y. -H., Yim, H. -S., Lee, C. -D. and Yeo, I. -T., 2002, "Safe Arm Design for Service Robot," *In Proceedings of The Second IARP-IEEE/RAS Joint Workshop on Technical Challenge for Dependable Robots in Human Environments*, pp. 88~95, Toulouse, France.

Lim, H. -O. and Tanie, K., 2000, "Human Safety Mechanisms of Human-friendly Robots: Passive Viscoelastic Trunk and Passively Movable Base," *International Journal of Robotics Research*, Vol. 19, No. 4, pp. 307~335.

Lord Corporation, 1999, "Magnetorheological Fluid MRF-132LD," *Product Bulletin*.

Lord Materials Devision, 1999, "Magnetic Circuit Design," *Engineering Note*, November.

Morita, T. and Sugano, S., 1995, "Development of One-D.O.F. Robot Arm Equipped with Mechanical Impedance Adjuster," *Proc. of the IEEE/RSJ International Conference on Intelligent Robots and Systems*, pp. 407~412.

Morita, T., Suzuki, Y., Kawasaki, T. and Sugano, S., 1998, "Anticollision Safety Design and Control Methodology for Human-symbiotic Robot Manipulator," *Journal of the Robotics Society of Japan*, Vol. 16, No.1, pp. 102~109.

Oh, H. -U. and Onoda, J., 2002, "An Experimental Study of a Semiactive Magneto-rehological Fluid Variable Damper for Vibration Suppression of Truss Structures," *Smart Materials and Structures*, Vol. 11, pp. 156~162.

Society of Automotive Engineers, 1999, "Human Tolerance to Impact Conditions as Related to Motor Vehicle Design-SAE J885 Jul86," *SAE Handbook (SAE Information Report)*, Vol. 3, pp. 34.464~34.481.

Walker, I.D., 1994, "Impact Configurations and Measures for Kinematically Redundant and Multiple Armed Robot Systems," *IEEE Trans. Robotics and Automation*, Vol. 10, No. 5, pp. 670~683.

Yamada, Y., Suita, K., Imai, K., Ikeda, H. and Sugimoto, N., 1997, "Human-robot Contact in the Safeguarding Space," *IEEE/ASME Transactions on Mechatronics*, Vol. 2, No. 4, pp. 230~236.

Yoon, S. -S., Kang, S., Kim, S. -J., Kim, Y. -H., Yim, H. -S. and Kim, M., 2002, "Design and Control of a Passive Compliant Joint for Human-friendly Service Robots," *International Conference on Control, Automation and Systems*, CD-ROM.

Yoshida, K., Mavroidis, C. and Dubowsky, S., 1995, "Experimental Research on Impact Dynamics of Spaceborne Manipulator Systems," *Preprints of the Fourth Int. Symp. On Experimental Robotics, ISER 95*, Stanford, California, pp. 271~277.